J Comput Neurosci (2009) 26:91–107
DOI 10.1007/s10827-008-0100-z

A computational modelling approach to investigate different targets in deep brain stimulation for Parkinson's disease

Marco Pirini · Laura Rocchi · Mariachiara Sensi · Lorenzo Chiari

Received: 30 July 2007 / Revised: 18 March 2008 / Accepted: 13 May 2008 / Published online: 14 June 2008

Abstract We investigated by a computational model of the basal ganglia the different network effects of deep brain stimulation (DBS) for Parkinson's disease (PD) in different target sites in the subthalamic nucleus (STN), the globus pallidus pars interna (GPi), and the globus pallidus pars externa (GPe). A cellular-based model of the basal ganglia system (BGS), based on the model proposed by Rubin and Terman (J Comput Neurosci 16:211–235, 2004), was developed. The original Rubin and Terman model was able to reproduce both the physiological and pathological activities of STN, GPi, GPe and thalamo-cortical (TC) relay cells. In the present study, we introduced a representation of the direct pathway of the BGS, allowing a more complete framework to simulate DBS and to interpret its network effects in the BGS. Our results suggest that DBS in the STN could functionally restore the TC relay activity, while DBS in the GPe and in the GPi could functionally over-activate and inhibit it, respectively. Our results are consistent with the experimental and the clinical evidences on the network effects of DBS.

Keywords Computational model · Basal ganglia · Parkinson's disease · Deep brain stimulation

Action Editor: David Terman

M. Pirini · L. Rocchi · L. Chiari (✉)
Biomedical Engineering Unit, Department of Electronics, Computer Science & Systems, Università di Bologna, Viale Risorgimento 2, 40136 Bologna, Italy
e-mail: lorenzo.chiari@unibo.it

M. Sensi
Department of Neuroscience, S. Anna University Hospital of Ferrara, Ferrara, Italy

1 Introduction

The basal ganglia system (BGS) is a group of four cerebral nuclei that receive information from the whole cortex and project mainly to the frontal cortex through the thalamus. The nuclei are the striatum, the substantia nigra (further divided in pars compacta, SNc, and pars reticulata, SNr), the subthalamic nucleus (STN), and the globus pallidus (further divided in pars interna, GPi, and pars externa, GPe). The striatum and the STN are considered the input ports of the BGS, while the GPi and the SNr are the output port of the BGS projecting to the thalamus and brainstem targets (DeLong and Wichmann 2007).

Parkinson's disease (PD) is a degenerative disease with cardinal motor symptoms that correlate with the loss of dopaminergic cells in the SNc. PD is characterized by akinesia, bradykinesia, rigidity, resting tremor at frequencies between 4 and 7 Hz, and other motor and postural impairments (Bergman and Deuschl 2002).

Ablative surgery of the thalamus or the GPi, pharmacological therapy based on levodopa (L-dopa), and deep brain stimulation (DBS) have been proved to be effective therapies for PD (Perlmutter and Mink 2006). DBS is a chronic electrical stimulation through electrodes implanted in the BGS or in the thalamus. DBS electrodes provide an high frequency (usually >100 pulses/s), continuous train of electrical pulses (Perlmutter and Mink 2006).

The GPi and the STN have been identified as sites in the BGS where DBS improves many axial and cardinal symptoms in patients affected by advanced PD (Burchiel et al. 1999; Yokoyama et al. 1999; Ostergaard and Sunde 2006). Quantitative studies showed that STN- and GPi-DBS improve advanced PD patients' stability in quiet stance (Rocchi et al. 2002; Maurer et al. 2003; Rocchi et al. 2004) and increase the step length and the speed of steady-state gait

(Faist et al. 2001; Defebvre et al. 2002; Rizzone et al. 2002; Ferrarin et al. 2004). STN-DBS is assumed to present a higher risk of dyskinetic side-effects than does GPi-DBS (Krack et al. 1999); thus, patients suffering predominantly from L-dopa-induced dyskinesia are commonly directed to GPi-DBS (Perlmutter and Mink 2006).

A recent analysis of patient outcomes (Weaver et al. 2005; Follett et al. 2005) highlighted how PD patients who had undergone STN-DBS and those who had undergone GPi-DBS experienced comparable improvements both in motor function and in performance of activities of daily living following surgery. In a multicenter study with a 4-year follow-up, PD patients who had undergone STN-DBS and those who had undergone GPi-DBS exhibited significant improvement in many cardinal features of PD, such as tremor, rigidity, bradykinesia, and tremor (Rodriguez-Oroz et al. 2005).

The GPe has been recently proposed as a DBS target for PD. Vitek et al. (2004) have shown that patients undergoing GPe-DBS improved more in terms of bradykinesia, akinesia, and rigidity than did patients undergoing GPi-DBS. GPe-DBS induced more dyskinetic events than did GPi-DBS.

Despite the paucity of data directly comparing different targets for DBS, many clinicians already consider the STN to be the preferred target site for PD, even though GPi (GPe) may be similarly effective (Vitek et al. 2004; Anderson et al. 2005). While comparative, blinded experimental studies are underway to compare the different DBS targets, we meant in this paper to give a contribution to elucidate the issue by means of a computational modelling approach of the BGS.

So far, most of the theoretical and computational models have been proposed to interpret both the role of the BGS in the CNS and the pathological behaviour of the BGS (mostly in PD) (see Humphries et al. 2006; Leblois et al. 2006; and DeLong and Wichmann 2007 for the most recent and complete modelling frameworks and for a brief review of the previously presented models).

The BGS plays a key role in the executive functions of the central nervous system (CNS). Briefly, the most accepted theory (action selection theory) about BGS states that it behaves as a selection system between competing motor and/or cognitive plans (Mink 1996; Beiser et al. 1997; Berns and Sejnowski 1998; Redgrave et al. 1999; Brown et al. 2004; Nambu 2004; DeLong and Wichmann 2007). In most of the models of the action selection mechanism in the BGS, the selection is performed in the striatum and the subsequent activation of the selected plan and the inhibition of the competing plans are performed through the so called "direct" (striatum → GPi → thalamus) and "indirect" (striatum → GPe → STN → GPi → thalamus) pathways.

In subjects affected by PD the neural activity in the nuclei of the BGS is severely altered, regarding both the mean firing rates and the discharge patterns of the neural populations (Raz et al. 2000; Brown et al. 2001; Bergman and Deuschl 2002); Several theoretical and computational models for PD have been proposed. Most of these models offer an explanation for PD in terms of: (a) alteration of the mean activities of the direct and of the indirect pathway (Delong 1990; Albin et al. 1995); (b) alteration of the discharge patterns of the BGS nuclei (Terman et al. 2002; Rubin and Terman 2004), (c) impairment of the striatal selectivity (Mink 1996; Humphries et al. 2006); and (d) a mix of the previous frameworks (Bar-Gad et al. 2003; Humphries et al. 2006; DeLong and Wichmann 2007).

The therapeutic action of DBS acts through mechanisms not yet completely clear (see Montgomery Jr and Baker 2000; Benabid et al. 2002; Dostrovsky and Lozano 2002; Vitek 2002; McIntyre et al. 2004; and Perlmutter and Mink 2006 for complete reviews of all the hypothesized mechanisms). Briefly, the problem involves three issues: (1) how does DBS influence the neuronal activity in the target site (local DBS effects)? (2) how do the local DBS effects influence the neuronal activity in the other structures in the CNS (network DBS effects)? and (3) why do the network DBS effects provide therapeutic effects?

BGS models were never used, to authors' knowledge, to compare the network effects of DBS in different targets in the BGS. To achieve this aim we needed a convincing BGS model having: (a) a theory about the physiological and the pathological (PD) functioning of the BGS and (b) a theory about the local DBS effects.

The model presented in this paper follows the seminal model by Rubin and Terman (2004) (RTM). The RTM is a model of the BGS that includes the STN, the GPi, the GPe, and the thalamus. Every nucleus is represented by a population of Hodgkin–Huxley cell models.

Rubin and Terman, through the RTM, provided a theory about the physio-pathological functioning of the BGS and about the network effects of the STN-DBS. In RTM, the thalamus is a simple relay station whose physiological role is to faithfully respond to the inputs arriving from the sensorimotor cortex (SMC). Thalamic cells receive also inhibitory inputs from the GPi cells. In the physiological state of the RTM the GPi activity is tonic and uncorrelated among subpopulations of the GPi cells and do not disrupt the thalamic relay activity. In the PD state of the RTM the GPi activity is phasic and correlated among subpopulations of the GPi cells and disrupt the thalamic relay activity. The PD GPi activity arise from upstream PD STN and GPe activities. The STN and GPe populations are arranged in a mutually coupled architecture. In the PD state of the RTM, a weakened intra-GPe connectivity and an augmented striatal inhibition to the GPe bring the GPe and the STN activities to be: (a) synchronous oscillatory (with GPe and STN cells showing bursts of action potentials (APs) at 4–7 Hz) and (b) correlated among GPe and STN subpopulations.

The theory about the physio-pathological functioning of the BGS provided by Rubin and Terman originated from the experimental work by Plenz and Kitai 1999. In this work, Plenz and Kitai demonstrated that, in an organotypic culture, the mutually coupled GPe and STN populations could generate oscillatory and synchronized activity. The theory agrees with *in-vivo* physiological studies, that proved an abnormal, high level of synchronization in and between the BGS nuclei in PD (Raz et al. 2000; Bergman and Deuschl 2002).

Rubin and Terman assumed a very simple representation of the local DBS effects. In RTM, every DBS pulse elicits an AP in every STN cell. The limits of this assumption will be further addressed in Section 4.

During DBS, the pathological, phasic STN activity is replaced by an abnormal, regular activity that is synchronized with the DBS pulses train. The regularization of the STN activity brings to a regularization of the GPe and GPi activities. Rubin and Terman hypothesized that the main network effect of STN-DBS in the RTM is to stabilize the GPi inhibitory input to the thalamus and to restore the thalamic relay activity. This conclusion is consistent with the theories on the network effects of DBS proposed by McIntyre et al. (2004) and DeLong and Wichmann (2007).

While modelling in detail the indirect pathway of the BGS, the RTM does not provide any representation of the direct pathway. No striatal input to the GPi is considered. Consequently, no functional striatal control of the GPi activity and, subsequently, of the thalamic relay activity is modelled. In the RTM, the role of the thalamic cells in the physiological state is simply to respond to SMC inputs. On the contrary, the action selection theory of the BGS states that the thalamic relay activity is controlled by the BGS and is dynamically released only for the execution of the selected motor or cognitive plan. Therefore, we decided to improve the RTM by including a representation of the striatal input to the GPi and, consequently, of the direct pathway of the BGS. In our opinion, this more complete model of the BGS may allow a better understanding of the network effects of DBS.

The aims of this study were: (a) to better understand the differential network effects of STN-, GPi-, and GPe-DBS by using an extended version of the RTM, the eRTM, and (b) to compare results with clinical and experimental evidences regarding STN-, GPi-, and GPe-DBS.

2 Methods

2.1 Software tools

The eRTM has been implemented with Matlab 7.04 and Simulink 6.1, on a PC platform (Pentium IV 2 GHz, 1 GB RAM).

2.2 Features of the eRTM

The eRTM, outlined in Fig. 1, extends the RTM mostly by introducing in the model the direct pathway. In the following, for the sake of clarity, we will simply refer to the model we used as eRTM.

The eRTM models the STN, the GPe, the GPi, and the thalamus by four populations of Hodgkin–Huxley, mono-compartmental cell models. Therefore, each cell is represented by a set of differential equations. The eRTM consists in a network of 16 STN, 16 GPe, 16 GPi, and two thalamocortical (TC) relay cells. The eRTM considers: (a) the inhibitory connections striatum → GPi (representing the direct pathway), striatum → GPe, GPe → GPe, GPe → STN, GPe → GPi, and GPi → thalamus and (b) the excitatory connections STN → GPe, STN → GPi, and cortex → thalamus.

Each STN, GPe, and GPi population is divided in two groups of eight cells each. Each GPe cell receives inhibitory input from three cells of its own group, randomly chosen, and receives excitatory input from three STN cells, randomly chosen among the entire STN population. Every STN cell receives inhibitory input from three GPe cells chosen among a matched group in the GPe. It follows that, from a functional point of view, the GPe population (but not the STN population) is divided into two parallel channels. This connectivity design aims to reflect the real connectivity observed (GPe) or hypothesized (STN) in the nuclei of the BGS (Bar-Gad et al. 2003). Every GPi cell receives inhibitory input from a corresponding GPe neuron and excitatory input from a corresponding STN neuron. Every TC cell receives inhibitory input from eight GPi cells. A single realisation of the connectivity scheme described above was considered in the following analyses.

The striatal inputs to the GPe and to the GPi are represented by constant currents directly injected into GPe and GPi cells.

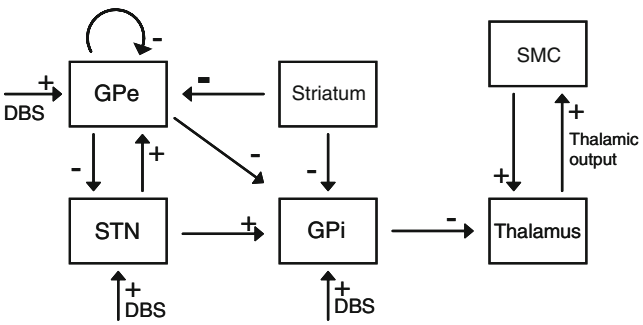

Fig. 1 Structures and connections in the eRTM model. *STN* Subthalamic nucleus, *GPe* globus pallidus pars externa, *GPi* globus pallidus pars interna, *SMC* sensorimotor cortex, *DBS* deep brain stimulation. DBS is alternatively applied in STN, GPe, or GPi in our simulations

The cortical excitatory inputs to TC cells are represented by a train of positive, rectangular current pulses directly injected into TC cells. Time intervals between subsequent pulses are selected from a Poisson distribution, with an enforced minimum interval of 10 ms, and determined as 10−log(ran(1))/0.03 ms, where ran(1) is a random number selected from a uniform distribution on [0, 1] (as in Rubin and Terman 2004).

See Rubin and Terman (2004) and Appendix for details on equations of the eRTM and parameter values.

2.3 Physiological and PD states

Two parameters were used to model the physiological and the PD state in the eRTM, according to Rubin and Terman (2004): (1) the indirect striatal current to GPe cells ($I_{\text{Striatum}\rightarrow\text{GPe}}$= 0 pA/μm^2 for the normal state, and $I_{\text{Striatum}\rightarrow\text{GPe}}$=−4 pA/μm^2 for the PD state) and (2) the intra-GPe inhibitory synaptic conductance ($g_{\text{GPe}\rightarrow\text{GPe}}$=0.3 nS/μm^2 for the normal state, and $g_{\text{GPe}\rightarrow\text{GPe}}$=0 nS/μm^2 for the PD state). The parameter changes turned out to be a good phenomenological model of dopamine depletion—by putting the model in the "correct" dynamic state for PD (see Section 3.1.4 and Fig. 4)—but for reasons unknown, as we currently have no data to support the changes. The increase in striatal current to the GPe for the PD state follows the models of PD that propose an "increased response to excitatory input" in the indirect pathway of the BGS due to the decreased activation of D2 receptors in the striatum (DeLong and Wichmann 2007). The decrease in the intra-GPe inhibitory synaptic conductance in the PD state was motivated in Rubin and Terman (2004) by some experimental results with rats (Stanford and Cooper 1999; Ogura and Kita 2000). These results showed in fact that enkephalin and dynorphin act pre-synaptically on GABAergic terminals in GP (the functional homologous of the GPe in rodents) to reduce GABA release, while Rubin and Terman implicitly assumed that an increased level of inhibition from the striatum to GP after PD-related dopaminergic denervation could be positively correlated with the release of enkephalin and dynorphin. However, it should be pointed out that no results has been so far provided to sustain the cited assumption.

It is worth mentioning that we did not include the striatal current to the GPi ($I_{\text{Striatum}\rightarrow\text{GPi}}$) in the set of parameters used to switch the eRTM between the normal and the PD states. This neglect could seem controversial, given the models of PD that propose a "decreased response to excitatory input" in the direct pathway of the BGS due to the decreased activation of D1 receptors in the striatum. However, since we aimed to include the action selection theory in the eRTM and the current $I_{\text{Striatum}\rightarrow\text{GPi}}$ was the key parameter in doing that (as shown in following sections), we preferred to define the "PD state" of the eRTM as a state showing just the pathological activities arising in the indirect pathway. Pathological features arising in the direct pathway and involving $I_{\text{Striatum}\rightarrow\text{GPi}}$ were introduced and discussed later, in Sections 4.3 and 4.4.

2.4 DBS modelling

In the eRTM, the DBS was modelled as a train of rectangular, positive-current pulses directly injected into the cells belonging to the target site. This DBS modelling is rather simplistic, since in the reality the response of a neuron to extracellular stimulation is very different from its response to intracellular stimulation (see Section 4). The pulse amplitude in DBS was set to 400 pA/μm^2, while pulse length was set to 0.15, 0.3, and 1.2 ms for STN, GPi and GPe stimulation, respectively. These values ensured a 1:1 ratio between DBS pulses and APs in the target structures.

DBS was always tested on the PD state of the eRTM.

2.5 Outcome measures and simulations

We defined two outcome measures for a given set of DBS target and parameters:

1. The mean firing rate (MFR) of the GPi, calculated as the average firing rate of the 16 GPi cells (APs revealed by a thresholding method; threshold set to −20 mV).
2. The percentage effectiveness score (ES%), defined as the percentage of correct thalamic responses to SM cortical inputs (averaged over the 2 TC cells). A thalamic AP was considered correct if it occurred within 6 ms after a SMC input. Summary ES% was the average of the ES% computed in 25 runs of the simulation.

We defined also an additional parameter to monitor the degree of synchrony amongst the activities of the GPi cells in the physiological and PD states, the Synchrony Index (SI). For every GPi cell i (i=1,…, 16), we detected the APs by a thresholding method (threshold set to −20 mV) and we derived an "activation function" simply by counting the APs in consecutive, non-overlapping windows of 30 ms each. Then, we calculated the correlation coefficient for each pair of activation functions (number of meaningful pairs $N_P=n\ (n-1)/2$, n=16) and tested for significant correlation with α=0.05 (function *corrcoef* in Matlab; see Matlab documentation for the details on the statistical test for correlation). The SI was calculated as the ratio between the number of pairs showing significant correlation (N_S) and the total number of pairs N_P. It has to be pointed out that when testing for significant correlation, we did not correct for false positives (i.e. Type I errors), of which one would naively expect to find about 0.05*120=6 for each

simulation. However, the expected false positive rate ((false N_S)/N_P) is a constant since: (a) all simulations involved the same number of comparisons, from time-series with the same length (30 ms windows over 1 s), and (b) we already assumed a normal distribution for action potential counts by taking the *p*-values from the *corrcoef* function in Matlab. So, if the expected false positive rate is a constant, then the SI scores are comparable between, e.g., normal and PD simulations because both SI scores should have roughly the same error. Anyway, future applications of the SI score will take into account a correction for false positives.

Using the eRTM, we investigated by simulations:

(a) The role of the direct striatal input to GPi, in the physio-pathologic states and during DBS. Different values of $I_{\text{Striatum}\rightarrow\text{GPi}}$ (from −13 to 3 pA/μm^2, see Appendix) were tested for 1 s. Positive, depolarizing values for an inhibitory current have no physiological meaning. We included them in our analysis just for the sake of completeness and as a way to control if the resting membrane potential of GPi cells (set arbitrarily by the parameter I_{moreGPi}, see Appendix) was calibrated at a plausible level to further allow the inclusion of the AS theory in the model ($I_{\text{Striatum}\rightarrow\text{GPi}}$ directly adds up to I_{moreGPi}, see Appendix). In these simulations, DBS frequency was set to 120 Hz.

(b) The role of the DBS frequency. Different DBS frequencies (30, 60, 90, 120, 150, 180 Hz) and different sites of stimulation (GPi, GPe, and STN) were tested for 1 s. $I_{\text{Striatum}\rightarrow\text{GPi}}$ was assumed equal to 0, −5, and −11 pA/μm^2 (in order to sample the range for this variable).

Outcome measures were computed discarding the first 300 ms of the simulations, to allow extinction of the initial transient phases.

3 Results

3.1 Qualitative evaluation of DBS network effects

Qualitative network effects of STN-, GPe-, and GPi-DBS in the eRTM are illustrated in the following subsections. The activity of representative STN, GPe, and GPi cells were considered. In these simulations we left unchanged from Rubin and Terman (2004) the parameters regarding connectivity to GPi and to Thalamus: $g_{\text{STN}\rightarrow\text{GPi}}$=0.3 nS/μm^2, $g_{\text{GPe}\rightarrow\text{GPi}}$=1 nS/μm^2, $g_{\text{GPi}\rightarrow\text{Thalamus}}$=0.08 nS/μm^2, and $I_{\text{Striatum}\rightarrow\text{GPi}}$=0 pA/μm^2.

3.1.1 DBS target site: STN

The network effects of STN-DBS are shown in Fig. 2(a).

For 30 Hz DBS, STN cells responded in a 1:1 ratio. GPe cells, excited by STN cells, fired at the DBS frequency. The resulting network contribution to GPi cells lead them to fire in burst mode, in triplets of APs, at a burst frequency of 30 Hz.

For 120 Hz DBS, STN and GPe cells still fired in a 1:1 ratio with the DBS stimuli; note that the duration and the

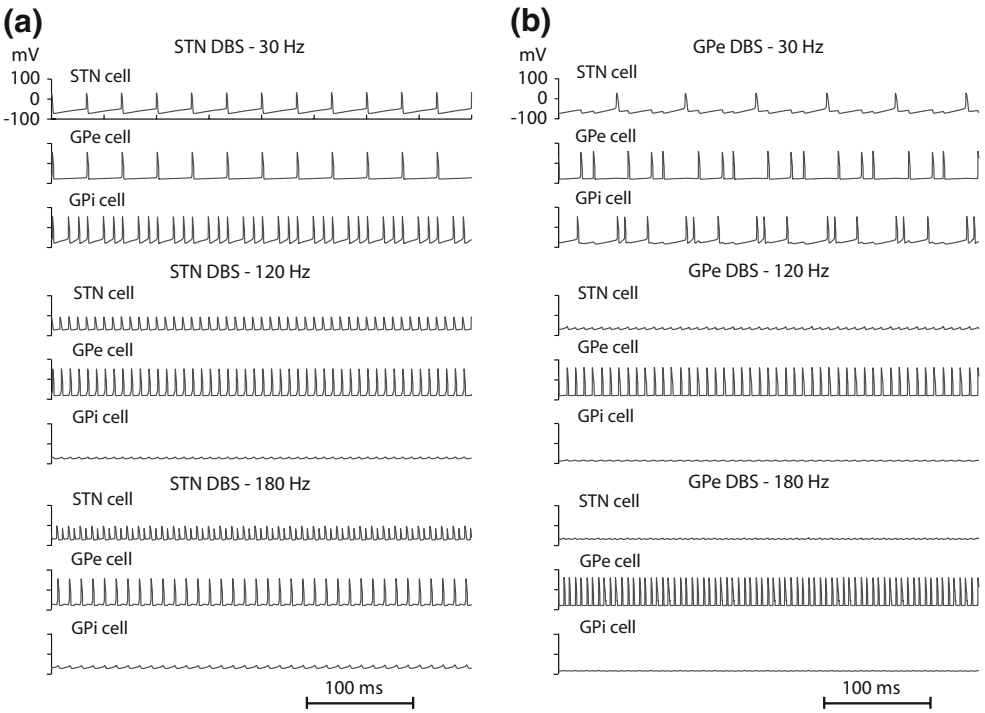

Fig. 2 Membrane potentials of one STN, one GPe, and one GPi cell during STN- (**a**) and GPe- (**b**) DBS. DBS stimulation at 30, 120 and 180 Hz

amplitude of STN APs diminished. The total inhibition from GPe activity overrode the total excitation from the STN activity and GPi cells were completely inhibited by the inhibitory GPe activity.

For 180 Hz DBS, STN cells fired in a 1:1 ratio, but one in every two DBS stimuli occurred during the refractory period of the AP arising from the previous DBS pulse. The consequent 'reduced' AP was not capable of driving a GPe AP and GPe cells fired at 90 Hz. In any case, STN APs did not drive GPi APs, and the GPi cells were still inhibited as for 120 Hz DBS.

3.1.2 DBS target site: GPe

The network effects of GPe-DBS are shown in Fig. 2(b).

For 30 Hz DBS, GPe and GPi cells regularized their activities at 90 Hz, while driving STN activity at 15 Hz.

DBS at 120 and 180 Hz drove GPe cells to fire in a 1:1 ratio with DBS stimuli. STN and GPi cells were therefore completely inhibited by the tonic, high-frequency GPe activity.

3.1.3 DBS target site: GPi

The network effects of GPi-DBS are shown in Fig. 3.

Upstream, pathological STN and GPe activities were not changed by GPi-DBS.

DBS at 30 and 120 Hz led GPi cells to respond in a 1:1 ratio to stimuli. Note the residual phasic patterns that resulted from the upstream, pathological GPe and STN activities.

DBS at 180 Hz led to a complete override of the GPi phasic activity resulting from the upstream GPe and STN activities.

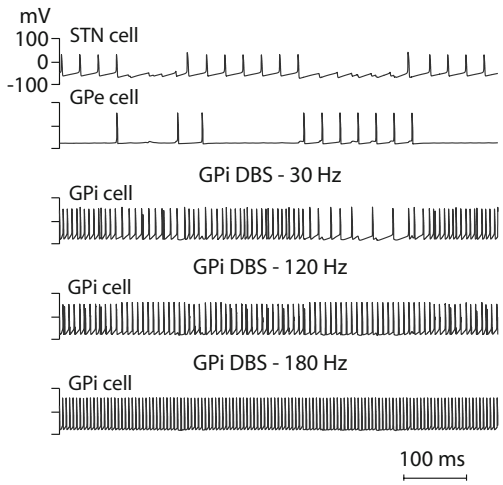

Fig. 3 Membrane potentials of one STN, one GPe, and one GPi cell during GPi DBS at 30, 120 and 180 Hz. STN and GPe cells are shown only once due to the fact that, in the eRTM, GPi DBS does not alter STN and GPe activity patterns

3.1.4 Thalamic activities in physio-pathological states and during DBS

Thalamic activity and the inhibitory contribution GPi → Thalamus are illustrated in Fig. 4 for different states of the eRTM: (a) physiological, (b) pathological (PD), (c) STN-/GPe-DBS at 120 Hz, and (d) GPi-DBS at 120 Hz.

In the physiological state, the GPi inhibitory contribution to the TC cells acts like a "white noise", whose level does not corrupt the TC relay activity.

In the PD state, the phasic activity of GPi cells leads to a phasic inhibitory contribution to the TC cells. The amplitude of the high-activity phases of this contribution is high enough to inhibit TC relay activity and to enhance TC rebound bursting during the following low-activity phases (see Rubin and Terman 2004, for the explanation of rebound bursting phenomena in TC cells).

STN- and GPe-DBS stabilize the GPi → Thalamus contribution at a low level (a single set of outputs was provided since the GPi activity was equal to 0 for both STN- and GPe-DBS in these simulations). A functional restoration of TC relay activity follows.

GPi-DBS stabilizes the GPi → Thalamus contribution at a high level. A functional inhibition of TC relay activity follows.

It should be pointed out that we found that the effect of STN-DBS on GPi-MFR and TC activity level is rather sensitive to DBS frequency between 100 and 150 Hz, even if, for the sake of clarity, we did not mention this point so far. It will be further discussed in Section 4.

3.2 Derived methods. Sensitivity analysis to the $g_{GPe \rightarrow GPi}$ and $g_{GPi \rightarrow Thalamus}$ parameters on the input–output relationships of the eRTM

Qualitative results on the network effects of STN- and GPe-DBS indicate that the relative weights of the STN → GPi and GPe → GPi connections may play a role in modulating the downstream effects of STN- and GPe-DBS. In fact, in a recent study on the RTM model (Pascual et al. 2006), the researchers eliminated the GPe → GPi connection to allow the STN activity during STN-DBS to drive GPi activity. Rubin and Terman (2004) showed that STN activity during STN-DBS drives GPi cells activity, but at a lower frequency than DBS frequency.

Another critical point emerging from qualitative results presented above is that the TC relay activity in the physiological state is substantially activated with $I_{Striatum \rightarrow GPi}=0$ pA/μm^2. This result is not consistent with the AS scenario, since an activation of the striatum (negative values for $I_{Striatum \rightarrow GPi}$) would inhibit the GPi and further enhance the TC relay activity. For the eRTM to be consistent with the AS theory (primarily in the physiological state), the TC relay activity should be inhibited with $I_{Striatum \rightarrow GPi}=0$ pA/μm^2 and progressively enhanced along with an increase of $|I_{Striatum \rightarrow GPi}|$.

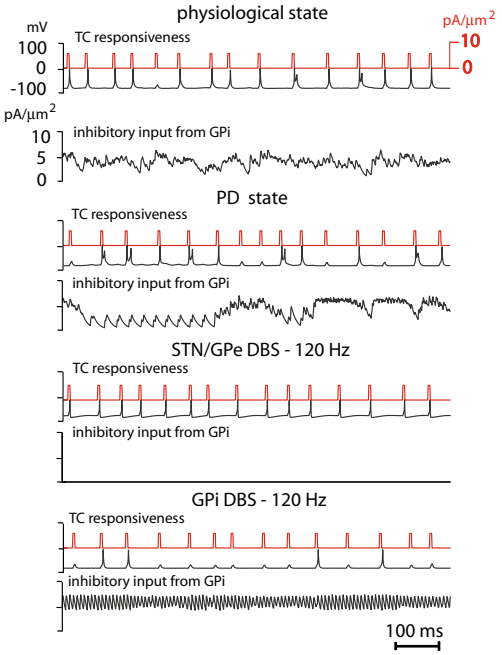

Fig. 4 Membrane potential of one Thalamo-cortical (TC) relay cell in response to SMC inputs (*upper panels*) and inhibitory inputs from the GPi layer (*lower panels*) in four different conditions. From *top* to *bottom*: physiological, PD, STN/GPe DBS—120 Hz, and GPi DBS—120 Hz

It should be noted that, in this context, the GPi → Thalamus inhibitory conductance may play an important role.

Having these issues in mind, we decided to perform a preliminary sensitivity analysis to the parameters $g_{GPe\rightarrow GPi}$ and $g_{GPi\rightarrow Thalamus}$ on the input–output relationships between the striatal input to GPi (input) and the TC relay activity (output) (leaving unchanged the upstream STN/GPe module of the eRTM and the $g_{STN\rightarrow GPi}$ parameter). We tested the following states of the model: (a) physiological, (b) PD, (c) STN-DBS at 120 Hz, (d) GPe-DBS at 120 Hz, and (e) GPi-DBS at 120 Hz. The tested values for the two parameters were: (a) 0, 0.3, 0.5, 0.7, and 1 nS/μm^2 for $g_{GPe\rightarrow GPi}$, and (b) 0.08, 0.16, and 0.24 nS/μm^2 for $g_{GPi\rightarrow Thalamus}$ (original values in the RTM: $g_{GPe\rightarrow GPi}$=1 nS/μm^2; $g_{GPi\rightarrow Thalamus}$= 0.08 nS/μm^2). The aim of this analysis was to determine the optimal values for the two parameters allowing (a) a proper integration of the AS theory in the eRTM, and (b) a consequent better explanation of the network effects of DBS on different targets. States of the model, simulations, values for $I_{Striatum\rightarrow GPi}$, and outcome measures were defined, run, and determined as described in Sections 2.3 and 2.5.

3.3 Derived results. Sensitivity analysis to the $g_{GPe\rightarrow GPi}$ and $g_{GPi\rightarrow Thalamus}$ parameters on the input–output relationships of the eRTM

Figures 5, 6, 7, 8 and 9 show the results of the sensitivity analysis, each one for a given value of $g_{GPe\rightarrow GPi}$. In each figure, panel (a) shows GPi-MFR in the five states of the eRTM as a function of $I_{Striatum\rightarrow GPi}$ and SI for the physio-pathological states (SI are given as mean ± standard deviation, since different values arise from different values of $I_{Striatum\rightarrow GPi}$). Panels (b), (c), and (d) show ES% as a function of $I_{Striatum\rightarrow GPi}$ for different values of $g_{GPi\rightarrow Thalamus}$ (0.08, 0.16, and 0.24 nS/μm^2, respectively).

3.4 DBS network effects: influence of DBS frequency

Figure 10 shows GPi-MFR (left panels), and ES% (right panels) for physio-pathological states of the eRTM and for DBS on different targets as a function of DBS frequency. In these simulations, $g_{GPe\rightarrow GPi}$ was set to 0.5 nS/μm^2 and $g_{GPi\rightarrow Thalamus}$ was set to 0.16 nS/μm^2 (see the Section 4 for

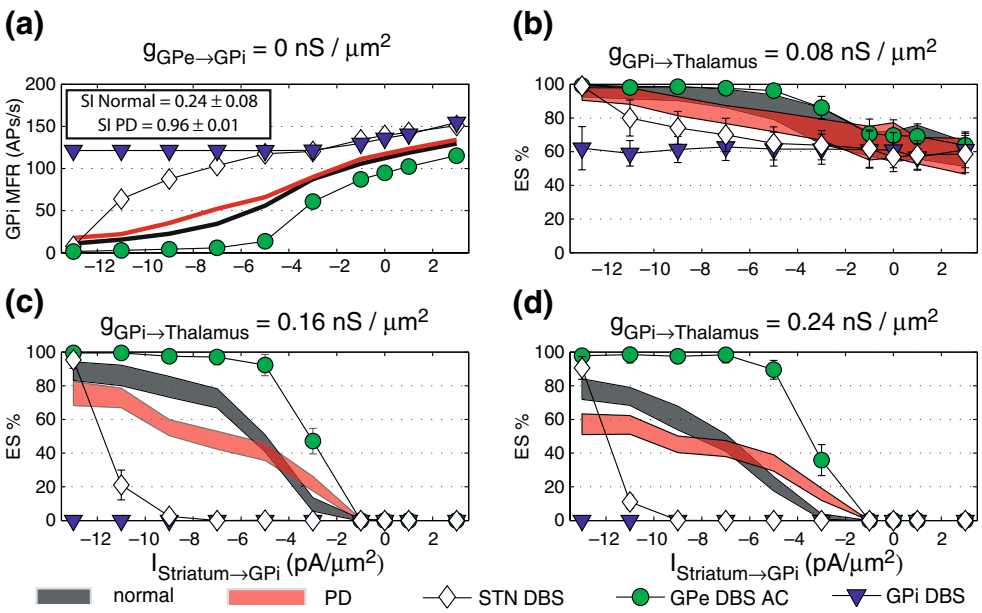

Fig. 5 Mean firing rate (*MFR*) of GPi (**a**), synchrony index values ((**a**), mean ± SD) and percentage of effectiveness score (*ES%*) for different values of $g_{GPi\rightarrow Thalamus}$ ((**b**), (**c**), and (**d**)), evaluated in different states of the eRTM and for different values of $I_{Striatum\rightarrow GPi}$. *Error bars* in (**b**), (**c**), and (**d**) refer to mean ± SD. These results were obtained with DBS frequency=120 Hz and $g_{GPe\rightarrow GPi}$=0 nS/μm^2

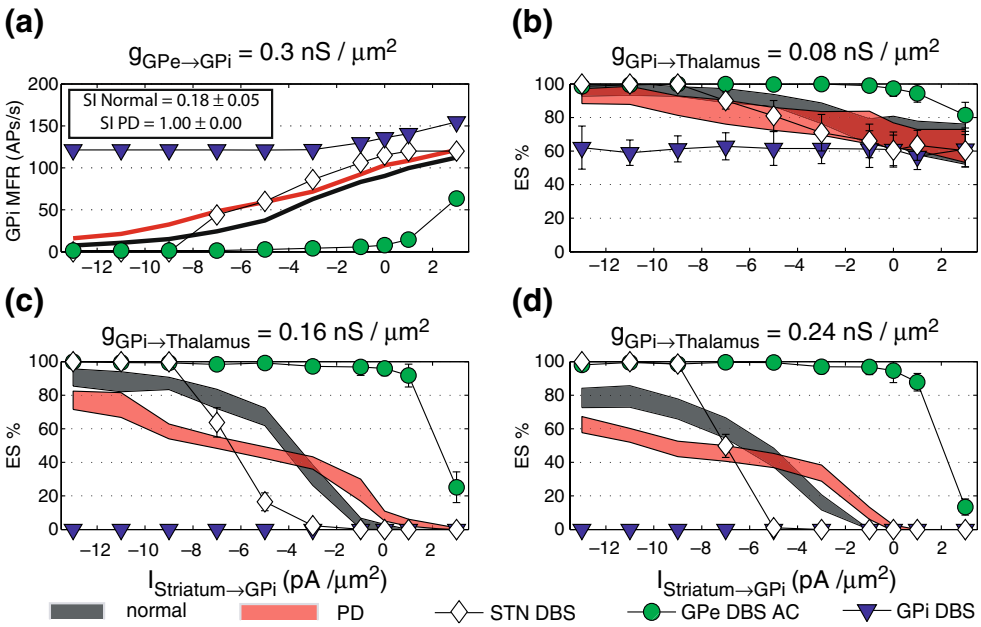

Fig. 6 Mean firing rate (*MFR*) of GPi (**a**), synchrony index values ((**a**), mean ± SD) and percentage of effectiveness score (*ES%*) for different values of $g_{GPi\rightarrow Thalamus}$ ((**b**), (**c**), and (**d**)), evaluated in different states of the eRTM and for different values of $I_{Striatum\rightarrow GPi}$. *Error bars* in (**b**), (**c**), and (**d**) refer to mean ± SD. These results were obtained with DBS frequency=120 Hz and $g_{GPe\rightarrow GPi}$=0.3 nS/µm²

the justification of this choices). We tested three different values for $I_{Striatum\rightarrow GPi}$ (0, −5, and −11 pA/µm²).

4 Discussion

4.1 Evaluation of results

4.1.1 Input–output relationships and DBS network effects as functions of $g_{GPe\rightarrow GPi}$, $g_{GPi\rightarrow Thalamus}$ and stimulation site

In the action selection theory, the role of the direct pathway is to drive, in synergy with indirect and hyperdirect pathways, an optimal and selective activation of TC relays. Thus, the relay activity in a particular TC cell is absent until an action involving this TC relay is selected in the striatum. Striatal inhibitory input to GPi then increases, leading to a decrease of GPi activity and to a subsequent release from inhibition of the selected TC relay.

The variable $I_{Striatum\rightarrow GPi}$ (see Appendix) has been introduced in the eRTM to model the striatal input to the GPi due to the direct pathway, thus becoming the input variable of the control system modelled by the eRTM. GPi-MFR and ES% could then be considered as the output variables of the eRTM. The method used here to model the striatal input to the GPi (a simple constant current to GPi

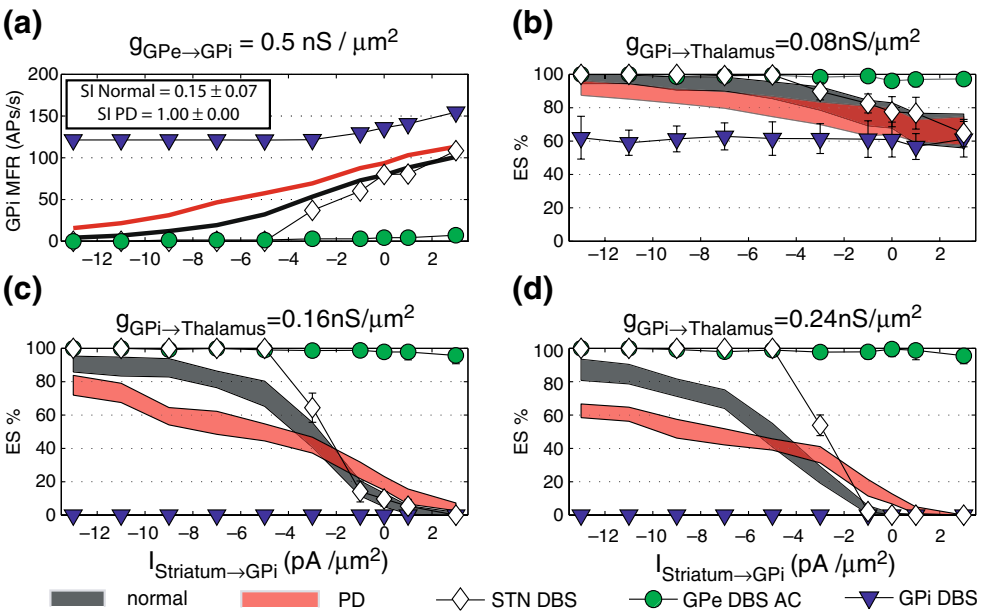

Fig. 7 Mean firing rate (*MFR*) of GPi (**a**), synchrony index values ((**a**), mean ± SD) and percentage of effectiveness score (*ES%*) for different values of $g_{GPi\rightarrow Thalamus}$ ((**b**), (**c**), and (**d**)), evaluated in different states of the eRTM and for different values of $I_{Striatum\rightarrow GPi}$. *Error bars* in panels (**b**), (**c**), and (**d**) refer to mean ± SD. These results were obtained with DBS frequency=120 Hz and $g_{GPe\rightarrow GPi}$=0.5 nS/µm²

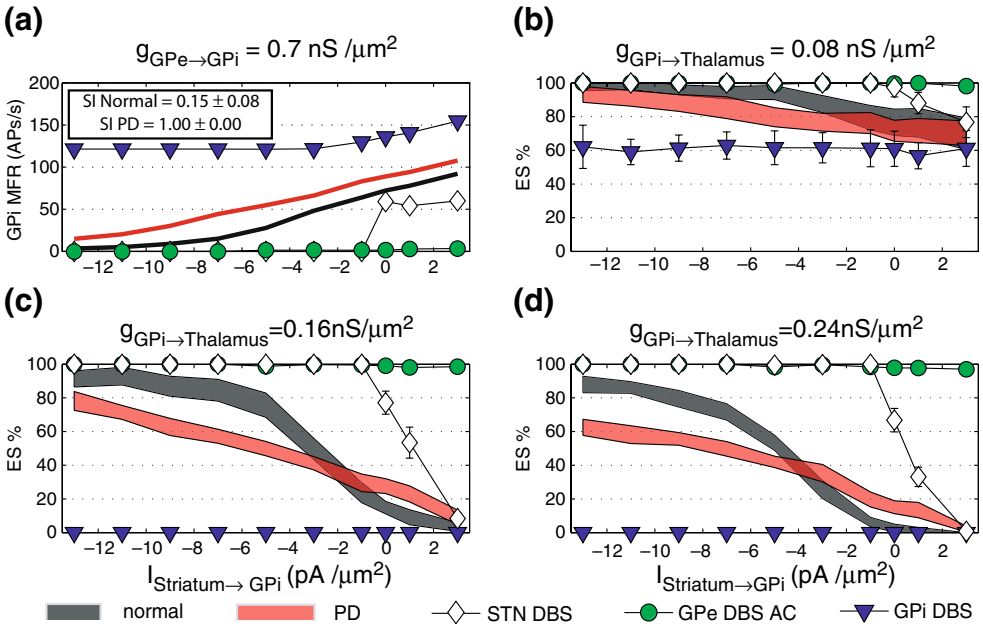

Fig. 8 Mean firing rate (*MFR*) of GPi (**a**), synchrony index values ((**a**), mean ± SD) and percentage of effectiveness score (*ES%*) for different values of $g_{GPi\rightarrow Thalamus}$ ((**b**), (**c**), and (**d**)), evaluated in different states of the eRTM and for different values of $I_{Striatum\rightarrow GPi}$. *Error bars* in (**b**), (**c**), and (**d**) refer to mean ± SD. These results were obtained with DBS frequency=120 Hz and $g_{GPe\rightarrow GPi}$=0.7 nS/μm²

cells) could not entirely capture its local effects on GPi, but could approximate its network effects on BGS.

As can be seen in Figs. 5, 6, 7, 8 and 9:

(a) GPi-MFR (panels (a)) increased monotonically for all the tested configurations of the eRTM and for all the tested values of $g_{GPe\rightarrow GPi}$ when $I_{Striatum\rightarrow GPi}$ was changed from −13 to 3 pA/μm².

(b) Mean SI (panels (a)) for the PD state was much higher than in the physiological state for all the tested values of $g_{GPe\rightarrow GPi}$. This result shows that the ability of the STN-GPe module of eRTM to spread PD patterns to the GPi is robust against changes in the GPe → GPi connectivity strength.

(c) Increasing $g_{GPe\rightarrow GPi}$ from 0 to 1 nS/μm² translated the GPi-MFR curves toward lower values in all the tested states of the eRTM, accordingly to the inhibitory nature of this connection. This effect was weaker (a) in the GPi-DBS state (GPi-DBS ensuring an *a-priori* activation of GPi at DBS frequency) and (b) in the GPe-DBS state (GPe-DBS ensuring a stable and robust inhibition of GPi—except for the case $g_{GPe\rightarrow GPi}$=0) as compared to the physio-pathological states. In the physiological state, the GPi-MFR range moved from [12 130] to [4/80] APs/s, while in the PD state the GPi-MFR range moved from [18 135] to [15 100] APs/s. The effect was much stronger in the STN-DBS state, as already partially seen in Section 3.1.1 and

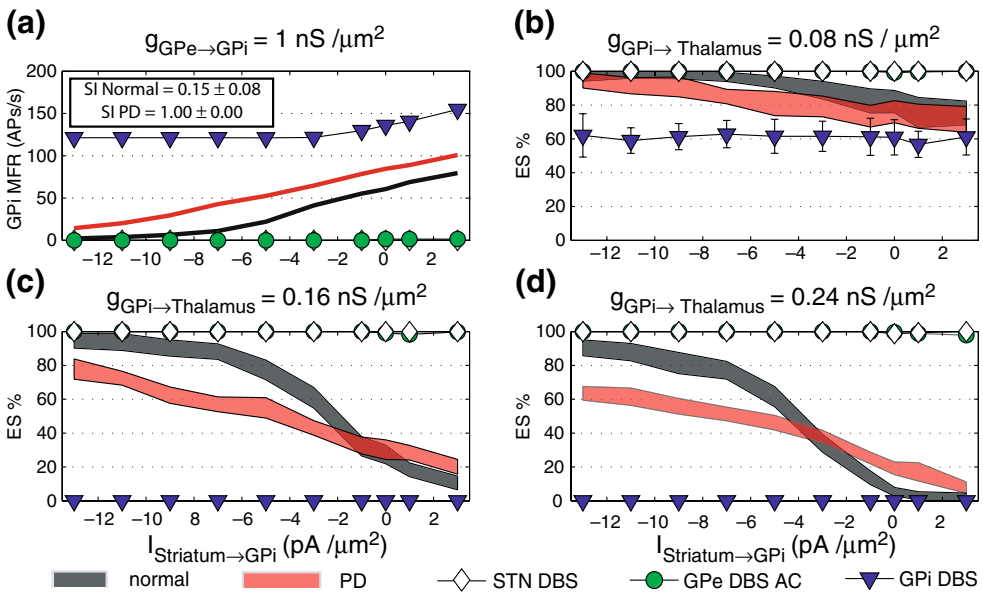

Fig. 9 Mean firing rate (*MFR*) of GPi (**a**), synchrony index values ((**a**), mean ± SD) and percentage of effectiveness score (*ES%*) for different values of $g_{GPi\rightarrow Thalamus}$ ((**b**), (**c**), and (**d**)), evaluated in different states of the eRTM and for different values of $I_{Striatum\rightarrow GPi}$. *Error bars* in (**b**), (**c**), and (**d**) refer to mean ± SD. These results were obtained with DBS frequency=120 Hz and $g_{GPe\rightarrow GPi}$=1.0 nS/μm²

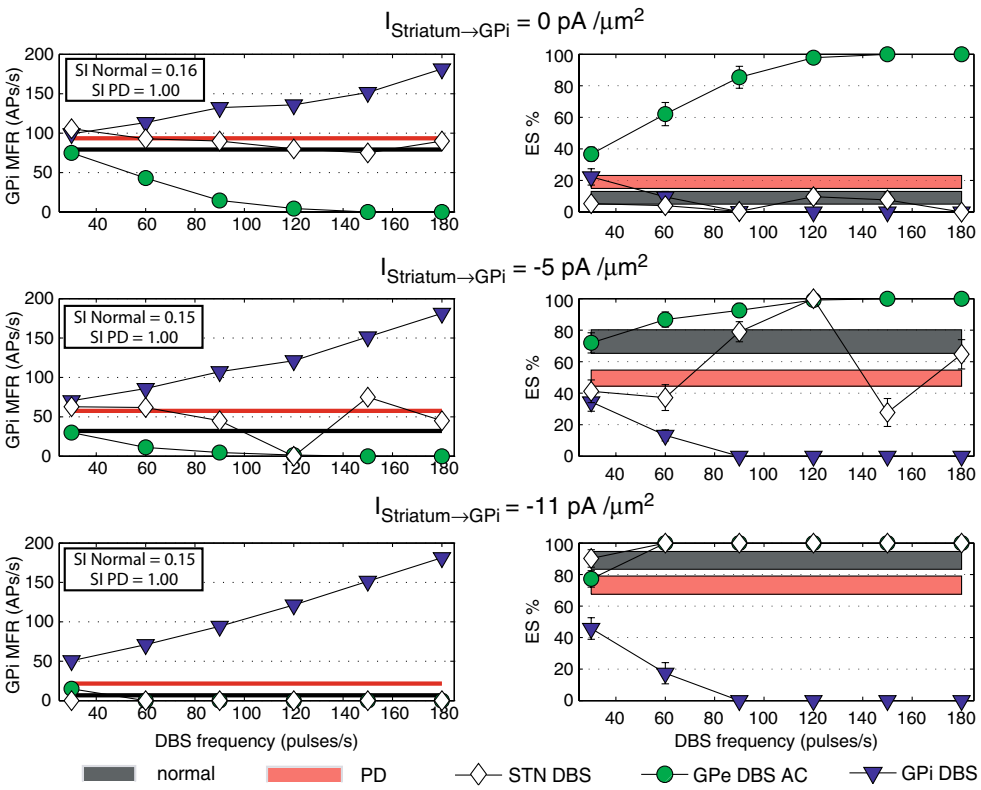

Fig. 10 Mean firing rate (*MFR*) of GPi, synchrony index values (*left panels*), and percentage of effectiveness score (*ES%*) (*right panels*), evaluated in different states of the eRTM, for different values of DBS frequencies, and for different values of $I_{Striatum \rightarrow GPi}$ (*upper panels*: 0 pA/µm^2; *middle panels*: −5 pA/µm^2; *lower panels*: −11 pA/µm^2). These results were obtained with $g_{GPe \rightarrow GPi}$= 0.5 nS/µm^2 and with $g_{GPi \rightarrow Thalamus}$=0.16 nS/µm^2

discussed in Section 3.2. Moving $g_{GPe \rightarrow GPi}$ from 0 to 1 nS/µm^2, the indirect GPe-driven inhibition of GPi subsequent to STN-DBS increasingly overrode the direct STN-driven excitation.

(d) ES% (panels (b), (c), (d)) decreased monotonically (or remained stable) for all the tested configurations of the eRTM and for all the tested values of $g_{GPe \rightarrow GPi}$ and $g_{GPi \rightarrow Thalamus}$ when $I_{Striatum \rightarrow GPi}$ was moved from −13 to 3 pA/µm^2.

(e) Looking at the physiological state of eRTM, the value of 0.16 and 0.24 nS/µm^2 for $g_{GPi \rightarrow Thalamus}$ were appropriate values, since with these values the direct current $I_{Striatum \rightarrow GPi}$ modulated the ES% from ~10% ($I_{Striatum \rightarrow GPi}$=0 pA/µm^2) to ~90% ($I_{Striatum \rightarrow GPi}$= −13 pA/µm^2) for most of the $g_{GPe \rightarrow GPi}$ values, in agreement with the AS theory. In contrast, the value of 0.08 nS/µm^2 for $g_{GPi \rightarrow Thalamus}$ was not appropriate to allow AS theory to be included in the model (ES% for $I_{Striatum \rightarrow GPi}$=0 pA/µm^2 were too high, for every tested value of $g_{GPe \rightarrow GPi}$).

(f) The control mechanism described in point (e) was partially disrupted in the PD state, where ES% increased much more slowly than in the physiological state. The PD curves showed a decreased slope for a wide range of the $I_{Striatum \rightarrow GPi}$ values compared to the physiological curves, leading to (1) an incomplete activation of the TC relay for high $|I_{Striatum \rightarrow GPi}|$ values and to (2) an incomplete inhibition for low $|I_{Striatum \rightarrow GPi}|$ values. Our results showed that, in the eRTM framework: (a) the disruption of the control mechanism in the PD state is not, *per se*, a consequence of an increase of the GPi-MFR values compared to the physiological state (indeed, ES% curves for physiological and PD states crossed each other in most of cases, while GPi-MFR curves did not) and (b) the disruption of the control mechanism in the PD state could arise also from an increase in the synchrony amongst the GPi cells (reflected in an increase in SI values), thus confirming the results of Rubin and Terman (2004) in a broader scenario.

(g) The control mechanism described in point (e) was completely disrupted in the GPi-DBS state (ES% curves were almost always close to 0 for every value of $I_{Striatum \rightarrow GPi}$) and in the GPe-DBS state (ES% curves were close to 100 for almost every value of $I_{Striatum \rightarrow GPi}$). ES% values in the GPi-DBS state were different from 0 only for low $g_{GPi \rightarrow Thalamus}$ values. ES % values in the GPe-RTM state were different from 100 only for low $|I_{Striatum \rightarrow GPi}|$ values and for low $g_{GPe \rightarrow GPi}$ values (both factors allowing GPi-MFR being different from 0). Thus, GPi-DBS led to a functional inhibition of the TC relay activity, while GPe-DBS led to a functional over-activation.

(h) The control mechanism described in point (e) was potentially restored during STN-DBS. The condition for this functional restoration was to choose an appro-

priate value for $g_{GPe\rightarrow GPi}$ (the position of the strictly decreasing portion of the ES% curves in the STN-DBS were very sensitive to $g_{GPe\rightarrow GPi}$, for the reasons already explained in point (c)). Note also that ES% curves in the STN- and GPe-DBS states were steeper than in any other state.

For the reasons explained in points (e) and (h), we chose for the following analysis and discussions $g_{GPe\rightarrow GPi}$= 0.5 nS/μm^2 and $g_{GPi\rightarrow Thalamus}$=0.16 nS/μm^2. As can be seen in Fig. 7(c), this choice allowed (a) a proper integration of the AS theory in the eRTM and (b) a suitable explanation for the clinical effectiveness of STN-DBS (the latter being further discussed and justified in the following sections).

4.1.2 DBS network effects as functions of stimulation site and frequency

Simulation results (Fig. 10) indicated that:

(a) GPe- and GPi-DBS modulated the GPi-MFR at levels that could lead to a functional over-activation (GPe-DBS) or to a functional inhibition (GPi-DBS) of the TC relay activity. This 'polarization' effect toward complete or absent TC responsiveness to SMC stimuli (1) increased monotonically with the DBS frequency and (2) was only partially modulated by the level of striatal inhibition to GPi.

(b) The network effects of frequency STN-DBS on GPi-MFR and TC responsiveness are not so easy to interpret, due to the disynaptic (STN → GPi and STN → GPe → GPi) connectivity from STN to GPi.

STN-DBS allowed the overall recovery of the striatal control on the TC responsiveness for every tested DBS frequency (setting $I_{Striatum\rightarrow GPi}$ to 0 and −11 pA/μm^2 led to ES% curves close to 0 and 100, respectively, thus qualitatively recovering the relationship between ES% and $I_{Striatum\rightarrow GPi}$ found in the normal state). However, the recovery was heavily influenced by the DBS frequency, as can be inferred by the GPi-MFR and ES% curves with $I_{Striatum\rightarrow GPi}$=−5 pA/μm^2. During 30 Hz DBS, STN cells responded in a 1:1 ratio with DBS stimuli. GPe cells, excited by STN ones, fired at the DBS frequency. The resulting network contribution to GPi cells lead them to fire at 60 Hz (a couple of APs for every STN AP). During 60, 90, and 120 Hz, STN and GPe cells still fired in a 1:1 ratio with the DBS stimuli. However, the duration and the amplitude of STN APs diminished as the DBS frequency increased, leading (a) the total inhibition from GPe activity to progressively override the total excitation from the STN activity and (b) GPi cells to be completely inhibited by the GPe activity at 120 Hz. During 150 Hz DBS, one out of two DBS stimuli occurred during a refractory period of STN cells, leading to reduced STN APs that were strong enough to drive GPi APs but not GPe APs, thus allowing a GPi activity at 75 Hz. During 180 Hz DBS, STN and GPe cells still fired in a 1:1 and in a 1:2 ratio with the DBS stimuli, respectively. However, the duration and the amplitude of STN APs diminished allowing the GPe activity to be more effective in inhibiting GPi cells, that fired at 45 Hz.

4.2 Simulation results and experimental evidence

The DBS frequency plays an important role in PD treatment. Usually, frequencies less than 100 Hz are thought to worsen PD symptoms, while frequencies greater than 100 Hz have been proven to have therapeutic benefits (Perlmutter and Mink 2006). Simulation results on the eRTM may provide a partial explanation of these clinical findings Low-frequency GPe- and GPi-DBS (e.g., 30 and 60 Hz) were not sufficient to drive the striatal control over the TC relay activity toward a functional over-activation (GPe-DBS), or a functional inhibition (GPi-DBS). Low-frequency STN-DBS was instead sufficient to drive a functional restoration of the control mechanism, but, interestingly, only high-frequency STN-DBS (90, 120, and 180 Hz, with the exception of 150 Hz) was able to restore the control mechanism in a limited range of $I_{Striatum\rightarrow GPi}$ ([0–5] pA/μm^2, instead of [0–11] pA/μm^2). A limited range of $I_{Striatum\rightarrow GPi}$ could be associated with PD, as explained in Sections 4.3 and 4.4. However, we did not deepen further this point in the present work.

Simulation results agree with experimental results about the DBS network effects achieved in human subjects and monkeys by microdialysis and extracellular recording procedures. Microdialysis evidences in PD subjects suggest that STN-DBS increases the STN activity (Stefani et al. 2005) and augments STN-driven excitation of GPi, while simultaneously decreasing GABA extracellular concentrations in the anteroventral thalamic motor nucleus, one of the thalamic nuclei targeted by GPi (Stefani et al. 2006). These speculations are confirmed by our simulation results, that suggest a simultaneous activation of STN and inhibition of GPi during STN-DBS. Indeed, GPi-MFR values were lower in the STN-DBS state than in the normal or PD ones for the physiological range of $I_{Striatum\rightarrow GPi}$ (Fig. 7(a)). Note that values for $g_{GPe\rightarrow GPi}$ lower than 0.5 nS/μm^2 would not allow this result (Figs. 5(a) and 6(a)).

Our findings are consistent also with results obtained by Kita and colleagues (Kita et al. 2005) on non-MPTP treated monkeys. In their work, single pulses and high-frequency stimulations (110 Hz) of STN evoked powerful excitatory responses in GPe neurons, while evoking a predominantly inhibitory response in GPi neurons. Their data suggest that

the STN → GPe excitatory response dominates the STN → GPe → GPe recurrent inhibition in the GPe, whereas the STN → GPe → GPi inhibitory response dominates the STN → GPi excitatory response in the GPi.

Hashimoto et al. (2003) and Kita et al. (2005) discussed the role of di-synaptic connectivity between STN and GPi, and both observed alternating phases of excitation and inhibition of GPi cells after every STN-DBS pulse. Simulation results on the network effects of STN-DBS at 120 Hz by using eRTM differed significantly from those obtained by Hashimoto et al. (2003). Their results suggested that GPi-MFR significantly increased during STN-DBS at 136 Hz. Results comparable to those from Hashimoto et al. (2003) were obtained in the eRTM by increasing the DBS frequency from 120 to 150 Hz (Fig. 10). Even if we did not conduct a complete input–output analysis for that DBS frequency, the GPi-MFR value for STN-DBS with $I_{\text{Striatum}\rightarrow\text{GPi}}=-5$ pA/μm^2 (Fig. 10) suggests that GPi-MFR values in the STN-DBS state could be higher than in the normal or PD ones for a wide range of $I_{\text{Striatum}\rightarrow\text{GPi}}$ values.

Simulation results showed that GPi-DBS acted to: (a) stabilize the GPi → thalamus inhibition at a level that is as high as the DBS frequency and (b) progressively inhibit TC cells as DBS frequency increases (complete inhibition at 180 Hz). These results are consistent with those from Anderson et al. (2003) in an extracellular recording study in MPTP-treated monkeys, where GPi-DBS at 100 Hz inhibited or decreased the activity of most of the downstream thalamic cells.

4.3 The AS theory in the eRTM and the PD modification of striatal input to the GPi

It has been argued that a decrease in nigrostriatal dopamine after PD onset could affect the direct pathway of BGS in two ways: (1) by a net decrease in striatal input to the GPi mediated by striatal D1 receptors (Delong 1990 and Albin et al. 1995) and/or (2) by a lack of striatal selectivity, with a concomitant spreading of uncontrolled activation to BGS channels not involved in the selected action. The first hypothesis (modification of the basal level/range of striatal input to GPi in PD) is compatible with the eRTM, as shown below (the eRTM already takes into account two channels, with eight GPi cells and one TC cell each). The second hypothesis (lack of striatal selectivity) would require further improvements in the model by adding a striatal module to the eRTM.

We preliminarily explored the first hypothesis by simulating a dynamical ON–OFF switching of the two channels in the eRTM. Figure 11 shows the experiment. Each channel was alternatively switched ON/OFF by a dynamical activation of the striatal current to the 8 GPi cells (only one per channel is shown) belonging to that channel. Thus, the relay activity to SMC inputs of the TC cell belonging to the channel was allowed/inhibited. In Fig. 11 the normal state of eRTM was simulated, and a wide, physiological range for $I_{\text{Striatum}\rightarrow\text{GPi}}$ was used ([0–11] pA/μm^2). In Fig. 12 we conducted an analogue analysis, but in the PD state of the eRTM and with a narrower range for $I_{\text{Striatum}\rightarrow\text{GPi}}$ ([0–5] pA/μm^2), thus simulating PD in both the indirect and in the direct pathway of the BGS. Note the disrupted striatal control on the TC relay activity due to the burst activities of GPi cells. Figure 13 shows the same experiment, but with STN-DBS at 120 Hz. The striatal control on the TC relay activity was fully recovered, even if the range for $I_{\text{Striatum}\rightarrow\text{GPi}}$ was still [0–5] pA/μm^2.

Figures 11, 12 and 13 qualitatively show in a dynamical experiment: (a) the full compatibility of the AS theory with the eRTM, (b) the static results already shown in Fig. 7(c), and (c) the short duration of the transient phases in the GPi-MFR and the TC relay activities against dynamical changes of the striatal input to GPi.

A full understanding of the therapeutic effects of DBS should take into account concomitant pharmacological treatment with L-dopa. The eRTM allows for the modelling of L-dopa consumption, by assuming that L-dopa simply acts to increase the basal level/range of striatal input to GPi (qualitative elements for a discussion on this issue are presented in the next section). The effects of L-dopa on the striatal selectivity would need further improvements in the eRTM to be modelled.

4.4 DBS sites: clinical outcomes versus simulation results

In clinical practice, the preferred surgical target for DBS in the treatment of PD is the STN (Weaver et al. 2005; Follett et al. 2005). However, results from randomized studies (Burchiel et al. 1999; Anderson et al. 2005; Rodriguez-Oroz et al. 2005; Weaver et al. 2005; Follett et al. 2005) recently showed that both STN and GPi are effective DBS targets, leading to a renewed interest in GPi as a DBS target for PD (Okun and Foote 2005) and to the creation of other randomized studies (Follett et al. 2005; Weaver et al. 2005).

As stated before, our simulation approach: (a) outlines three different network effects that could be associated with STN-, GPe-, and GPi-DBS and (b) qualitatively allows the modelling of the AS mechanism (in both normal and PD state of the eRTM) and of the L-dopa consumption by assuming they act by modifying the basal level/range of striatal current to the GPi. Consequently, within the eRTM we could relate: (a) bradykinetic and akinetic aspects of PD—to the poor thalamic responsiveness (due to the PD state plus a reduced range of striatal current to the GPi); (b) dyskinetic events in PD—to the non-zero thalamic activation in the OFF state of a given channel and to the phasic noise induced

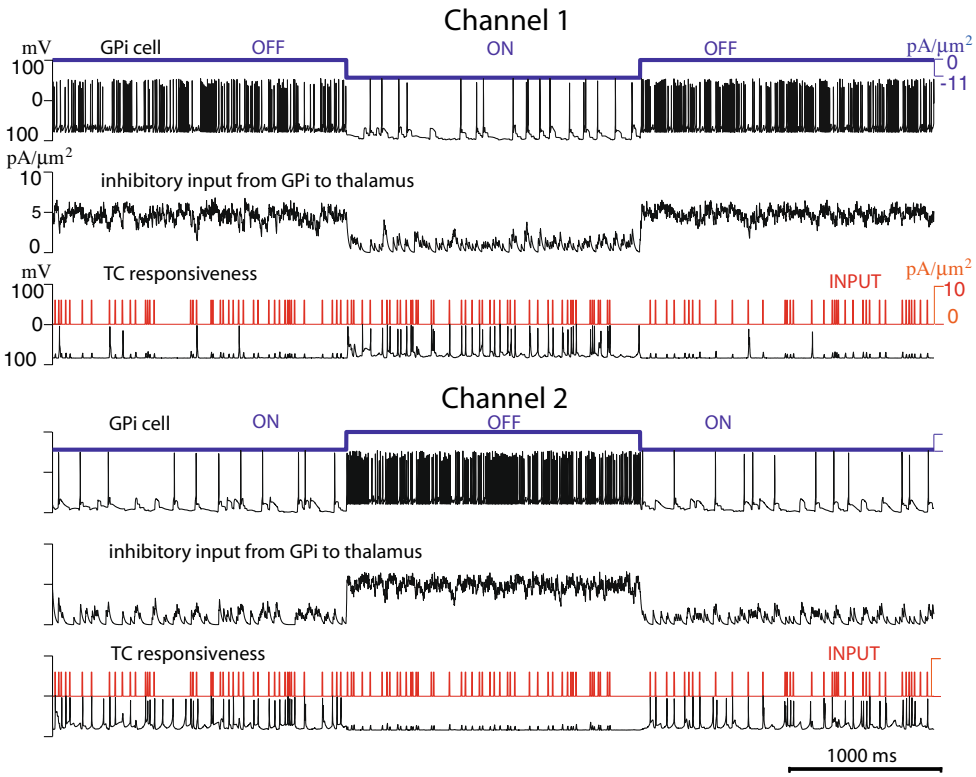

Fig. 11 Membrane potential of one GPi cell (*in black*) in response to dynamic striatal control (*in blue*) (*upper panels*), inhibitory inputs from the GPi to the TC relay cell (*middle panels*), and membrane potential of one TC cell (*in black*) in response SMC inputs (*in red*) in two different channels of the eRTM (*lower panel*). These results were obtained in the normal state of the eRTM, with $g_{GPe \rightarrow GPi}$= 0.5 nS/µm^2, with $g_{GPi \rightarrow Thalamus}$= 0.16 nS/µm^2, and with a [0–11] pA/µm^2 range for the striatal control

through the indirect pathway on the GPi activity; (c) benefits from L-dopa consumption—to a static increase of the range of striatal current to the GPi; and (d) dyskinetic events related to L-dopa consumption—to dynamical, uncontrolled modifications in the basal level/range of striatal current to the GPi (leading to uncontrolled activation of the thalamus).

We will read here our results from simulations using eRTM in the light of the few elements that the clinical

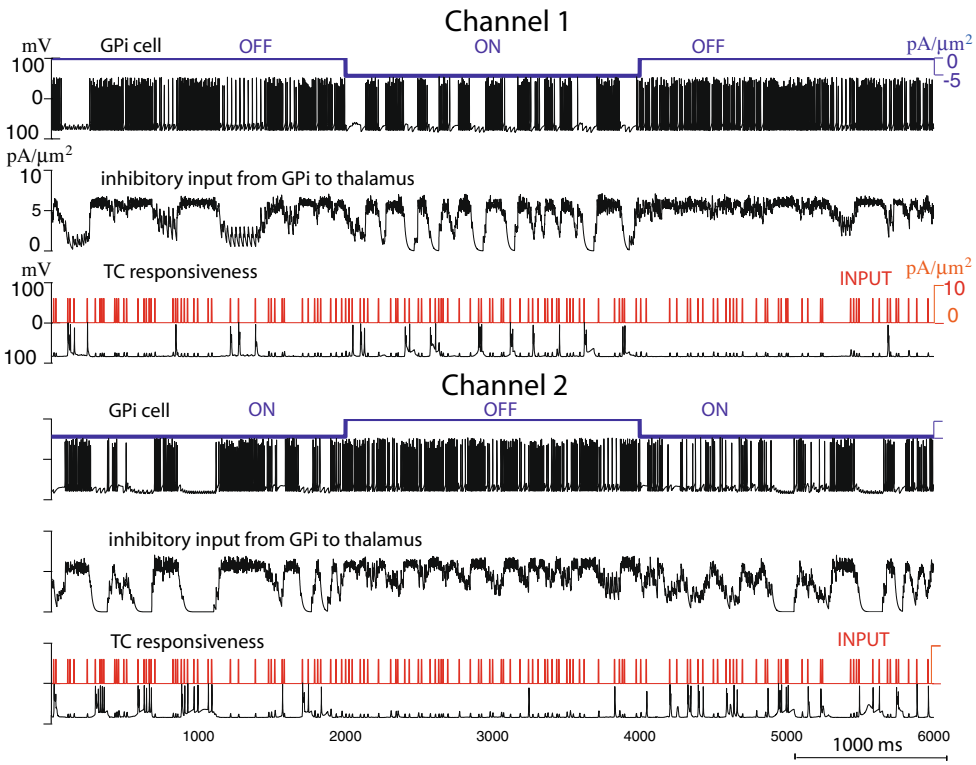

Fig. 12 Membrane potential of one GPi cell (*in black*) in response to dynamic striatal control (*in blue*) (*upper panels*), inhibitory inputs from the GPi to the TC relay cell (*middle panels*), and membrane potential of one TC cell (*in black*) in response SMC inputs (*in red*) in two different channels of the eRTM (*lower panel*). These results were obtained in the PD state of the eRTM, with $g_{GPe \rightarrow GPi}$=0.5 nS/µm^2, with $g_{GPi \rightarrow Thalamus}$=0.16 nS/µm^2, and with a [0–5] pA/µm^2 range for the striatal control

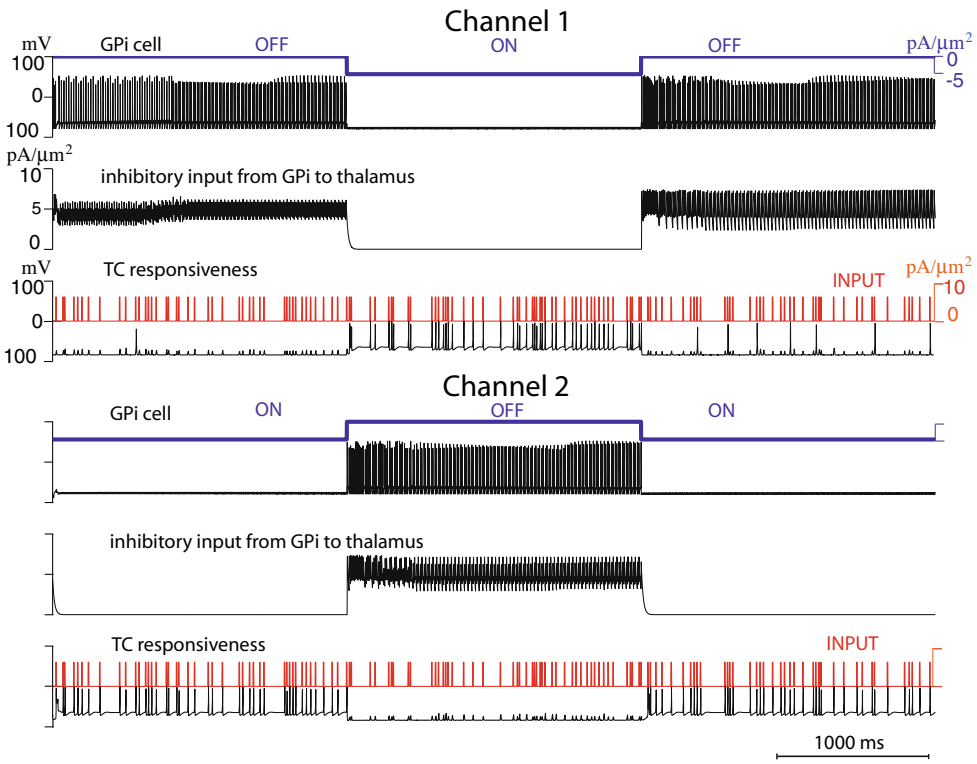

Fig. 13 Membrane potential of one GPi cell (*in black*) in response to dynamic striatal control (*in blue*) (*upper panels*), inhibitory inputs from the GPi to the TC relay cell (*middle panels*), and membrane potential of one TC cell (*in black*) in response SMC inputs (*in red*) in two different channels of the eRTM (*lower panel*). These results were obtained in the STN-DBS state of the eRTM, with a DBS frequency of 120 Hz, with $g_{GPe \rightarrow GPi}$= 0.5 nS/µm^2, with $g_{GPi \rightarrow Thalamus}$=0.16 nS/µm^2, and with a [0 –5] pA/µm^2 range for the striatal control

literature provides as distinctive of STN, GPe, and GPi targets or as part of the common expert clinical judgement in the decision about the preferred surgical target for a specific PD patient.

The functional inhibition of TC relay activity that we observed as a result of the high frequency GPi-DBS could be the responsible for the larger control of dyskinesia observed by skilled surgeons in GPi-DBS. Are wide and rapid fluctuations in striatal dopamine (and, consequently, in striatal input to GPi) due to L-dopa consumption in the advanced stages of PD neutralized by this functional inhibition? Our results could suggest that GPi is an ideal target for patients mostly impaired by hyperkinetic signs of PD.

The eRTM does not clarify why a complete inhibition of the TC relay activity due to GPi-DBS would bring to clinical benefits for PD patients. However, the cortex → BGS → thalamus → cortex loop is not the unique anatomical and functional circuit in the central nervous system devoted to the movement control. Other circuits, and primarily the cortex → cerebellum → thalamus → cortex, are involved in the motor control and co-control the thalamic activity. Lewis et al. (2007) have recently shown in a fMRI study on twins clinically discordant for PD that, despite some degree of functional segregation, these two circuits are functionally-related and task-specifically influenced by PD and L-dopa consumption. We could speculate that a regular, tonic output of the GPi (forced by GPi-DBS) is less disrupting the other circuits that control the thalamic activity than an irregular, bursty output, thus leading to clinical benefits. However, this hypothesis remains to be tested in a more complete model for the motor control, which should include the other circuits cited above.

Several comparative studies of STN- and GPi-DBS reported that patients undergoing GPi-DBS still received a larger daily L-dopa dose than those undergoing STN-DBS (Anderson et al. 2005; Ostergaard and Sunde 2006). The functional restoration of the striatal control of the TC relay activity that we observed as a result of the high-frequency STN-DBS could be the responsible for this reduced need of L-dopa in patients undergoing STN-DBS.

Bradykinesia tends to improve more with STN- than with GPi-DBS (Ostergaard and Sunde 2006). Based on our results, we hypothesize that STN stimulation speeds up the execution of movements and that STN could be an ideal target for patients mostly impaired by hypokinetic signs of PD.

Finally, it has been observed that GPe-DBS improves bradykinesia and akinesia compared to GPi-DBS and that GPe-DBS induces more dyskinetic events than GPi-DBS (Vitek et al. 2004). This observation is consistent with the "always on" activation of the thalamus due to GPe-DBS.

See Fig. 14 for a resume of the points discussed above.

4.5 Limitations in the eRTM Model

In order to allow the building of more controllable, larger network models of the BGS, we think that future improve-

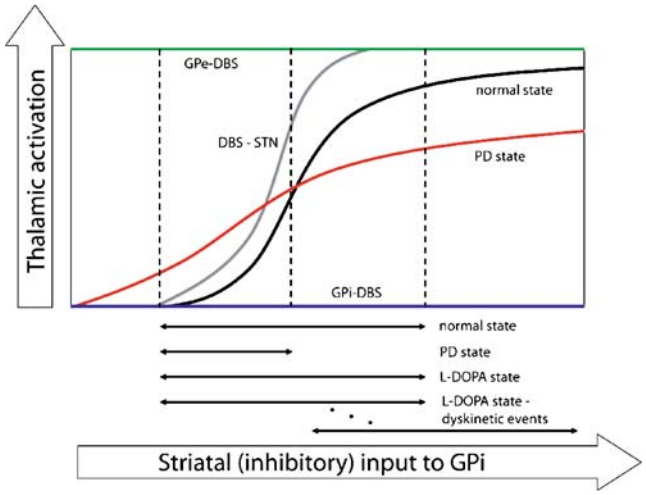

Fig. 14 Schematic representation of the possible input–output relationships of a single channel in the eRTM. Both quantitative (arising from simulations) and qualitative (arising from the discussions) features have been reported. The figure depicts our hypotheses regarding the static (modelling PD and L-dopa consumption) and the dynamic (modelling L-dopa induced dyskinesias) modifications of the basal level/range of the striatal input to GPi

ments of the RTM and of the eRTM should consider simpler models of single cells, eventually derived from those that have been used in the eRTM so far.

Other limitations are discussed in the following.

(a) The eRTM incorporates a mono-compartmental cell representation. Consequently, there is a wide range of phenomena that has been proposed (see Benabid et al. 2002; Lozano et al. 2002; and McIntyre et al. 2004) to explain the local effects of extra-cellular stimulation that cannot be further investigated with the eRTM. These phenomena include: (1) differential effects varying electrode-to-neurons distance, (2) differential effects on somas, dendrites, and axons, (3) synaptic activation/inhibition effects, (4) neurotransmitters depletion, and (5) antidromic propagation of AP.

(a) Rubin and Terman assumed that the main local effect of DBS is that DBS pulses enhance firing in the target nuclei, and modelled DBS pulses by injecting a current in the cells of the target nuclei. We kept this simplification, even if it was found that, in most DBS configurations (varying across polarity and type of stimuli), DBS pulses may *inhibit* somas and dendritic trees while *exciting* efferent axons (see McIntyre et al. 2004). Since the main network effects of DBS are mediated by efferent axons in the eRTM, we considered acceptable the theory about the local effects of DBS proposed by Rubin and Terman. However, the findings by McIntyre et al. (2004) substantially limit any sensitivity analysis regarding variation in duration and amplitude of DBS pulses in the eRTM framework, since there are not direct relationships between these parameters in extracellular and intracellular stimulation protocols (McIntyre et al. 2004). This consideration explains why we did not repeat the sensitivity analysis on these DBS parameters performed in the original paper by Rubin and Terman and in a recent work on RTM by Feng et al. (2007).

(b) The RTM does not consider any possible functional encoding of information in the physio-pathological functioning of BGS. An improvement has been achieved in this work, by including some features (the direct pathway) of the action selection theory in the eRTM. The action selection mechanism was modelled just in the direct pathway, while it could involve also the indirect and the hyperdirect ones (as modelled in Humphries et al. 2006 and Leblois et al. 2006). The direct pathway was the first to be identified as a candidate neural substrate of the action selection mechanism, since it shows clear, funnel-like channel segregation among the nuclei it involves. Future improvements are needed, in order to include also functional representations of: (1) the indirect pathway (that is present in the eRTM, but only to explain the transition from the physiological to the PD states), (2) the hyperdirect pathway, and (3) the striatal selectivity.

(c) The results shown in this paper only pertain to a single realisation of the connectivity scheme in the eRTM, as in (Rubin and Terman 2004). Whereas we suspect (based on the analysis and results provided in Terman et al. 2002) that the qualitative properties of the results obtained in the physiological and in the PD states of the eRTM are robust to changes in its underlying network (especially in the mutually connected STN and GPe populations), nevertheless we should corroborate this hypothesis by further analysis.

5 Conclusions

We set a computational model of the BGS, the eRTM, to integrate the action selection theory by the modelling of the direct pathway and some adjustments in two connectivity parameters. Then, we used the eRTM to compare the different network effects of STN-, GPe-, and GPi-DBS for PD. Our findings suggest that (a) STN-DBS, (b) GPe-DBS, and (c) GPi-DBS could have three completely different network effects: (a) a functional restoration, (b) a functional over-activation, and (c) a functional inhibition of the TC relay activity, respectively.

Our results were consistent with the experimental evidences regarding STN- and GPi-DBS and with the few comparative clinical evidences regarding STN-, GPe-, and GPi-DBS. We further showed that even a simple improvement (the modelling of the direct pathway) of the seminal

RTM toward the action selection theory framework significantly increased the power of the model in terms of (a) ability to interpret the clinical and the experimental evidences and (b) possible further usability as a unique framework to explain not only the network effects of DBS but also the mixed network effects of DBS and L-dopa.

Acknowledgments The authors would like to thank Jonathan E. Rubin from the University of Pittsburgh and David Terman from the Ohio State University for their help in implementing their model, Mauro Ursino and Stefano Severi from the University of Bologna for helpful discussions on network and single-cell models, and two anonymous reviewers for their precious hints and suggestions.

Appendix

Basic sets of equations of the eRTM are presented here. See Rubin and Terman (2004) and Terman et al. (2002) for more details on parameters and equations used.

The membrane potential of each STN neuron obeys the current balance equation:

$$C_m V'_{STN} = -I_L - I_{Na} - I_K - I_T - I_{Ca} - I_{AHP} + \\ + I_{GPe\to STN} + I_{MoreSTN} + I_{DBS}$$

The model features: potassium and sodium spike-producing currents I_K *e* I_{Na}; a low-threshold T-type Ca^{2+} current (I_T); a high-threshold Ca^{2+} current (I_{Ca}); a Ca^{2+} activated, voltage-independent after-hyperpolarization K^+ current (I_{AHP}); and a leak current (I_L). These currents (for STN, GPe, GPi and thalamic cells) are described by Hodgkin–Huxley formalism. Constant, depolarizing current $I_{MoreSTN}$ were introduced in Rubin and Terman (2004) to simulate diffuse excitatory input from cortex to STN cells.

Models for single GPe and GPi cells are very similar:

$$C_m V'_{GPe} = -I_L - I_{Na} - I_K - I_T - I_{Ca} - I_{AHP} + \\ + I_{STN\to GPe} + I_{GPe\to GPe} + I_{striatum\to GPe} + I_{MoreGPe}$$

$$C_m V'_{GPi} = -I_L - I_{Na} - I_K - I_T - I_{Ca} - I_{AHP} + \\ + I_{STN\to GPi} + I_{GPe\to GPi} + I_{striatum\to GPi} + I_{MoreGPi} \\ + I_{DBS}$$

Constant, depolarizing currents $I_{MoreGPe}$ and $I_{moreGPi}$ were introduced to simulate more diffuse excitation from STN to pallidal cells than that reproducible by synaptic connections. $I_{striatum\to GPe}$ and $I_{striatum\to GPi}$ represent the constant inhibitory current input from striatum to pallidal cells.

Thalamo-cortical relay cells obey the following equation:

$$C_m V'_{TH} = -I_L - I_{Na} - I_K - I_T - I_{GPi} - I_{SM}$$

I_{SM} represents a train of rectangular depolarizing current pulses from the cortex, identified by pulse amplitude (6 pA/μm^2), pulse length (6 ms), and pulse repetition frequency.

Synaptic currents $I_{\alpha\to\beta}$ from α to β cells were modelled as follows:

$$I_{\alpha\to\beta} = g_{\alpha\to\beta} \cdot \left[V_\beta - E_{\alpha\to\beta}\right] \sum_j s^j_\alpha$$

The summation is taken over the presynaptic α cells.

The input currents to the cells are negative if inhibitory, positive if excitatory under the sign convention used here.

References

Albin, R. L., Young, A. B., & Penney, J. B. (1995). The functional-anatomy of disorders of the basal ganglia. *Trends in Neurosciences*, *18*, 63–64.

Anderson, M. E., Postupna, N., & Ruffo, M. (2003). Effects of high-frequency stimulation in the internal globus pallidus on the activity of thalamic neurons in the awake monkey. *Journal of Neurophysiology*, *89*, 1150–1160.

Anderson, V. C., Burchiel, K. J., Hogarth, P., Favre, J., & Hammerstad, J. P. (2005). Pallidal vs subthalamic nucleus deep brain stimulation in Parkinson disease. *Archives of Neurology*, *62*, 554–560.

Bar-Gad, I., Morris, G., & Bergman, H. (2003). Information processing, dimensionality reduction and reinforcement learning in the basal ganglia. *Progress in Neurobiology*, *71*, 439–473.

Beiser, D. G., Hua, S. E., & Houk, J. C. (1997). Network models of the basal ganglia. *Current Opinion in Neurobiology*, *7*, 185–190.

Benabid, A. L., Benazzous, A., & Pollak, P. (2002). Mechanisms of deep brain stimulation. *Movement Disorders*, *17*, S73–S74.

Bergman, H., & Deuschl, G. (2002). Pathophysiology of Parkinson's disease: From clinical neurology to basic neuroscience and back. *Movement Disorders*, *17*, S28–S40.

Berns, G. S., & Sejnowski, T. J. (1998). A computational model of how the basal ganglia produce sequences. *Journal of Cognitive Neuroscience*, *10*, 108–121.

Brown, J. W., Bullock, D., & Grossberg, S. (2004). How laminar frontal cortex and basal ganglia circuits interact to control planned and reactive saccades. *Neural Networks*, *17*, 471–510.

Brown, P., Oliviero, A., Mazzone, P., Insola, A., Tonali, P., & Di Lazzaro, V. (2001). Dopamine dependency of oscillations between subthalamic nucleus and pallidum in Parkinson's disease. *Journal of Neuroscience*, *21*, 1033–1038.

Burchiel, K. J., Anderson, V. C., Favre, J., & Hammerstad, J. P. (1999). Comparison of pallidal and subthalamic nucleus deep brain stimulation for advanced Parkinson's disease: Results of a randomized, blinded pilot study. *Neurosurgery*, *45*, 1375–1382.

Defebvre, L. J. P., Krystkowiak, P., Blatt, J. L., Duhamel, A., Bourriez, J. L., Perina, M., et al. (2002). Influence of pallidal stimulation and levodopa on gait and preparatory postural adjustments in Parkinson's disease. *Movement Disorders*, *17*, 76–83.

Delong, M. R. (1990). Primate models of movement-disorders of basal ganglia origin. *Trends in Neurosciences*, *13*, 281–285.

DeLong, M. R., & Wichmann, T. (2007). Circuits and circuit disorders of the basal ganglia. *Archives of Neurology*, *64*, 20–24.

Dostrovsky, J. O., & Lozano, A. M. (2002). Mechanisms of deep brain stimulation. *Movement Disorders*, *17*, S63–S68.

Faist, M., Xie, J., Kurz, D., Berger, W., Maurer, C., Pollak, P., & Lucking, C. H. (2001). Effect of bilateral subthalamic nucleus stimulation on gait in Parkinson's disease. *Brain*, *124*, 1590–1600.

Feng, X. J., Shea-Brown, E., Greenwald, B., Kosut, R., & Rabitz, H. (2007). Optimal deep brain stimulation of the subthalamic nucleus—A computational study. *Journal of Computational Neuroscience*, *23*, 265–282.

Ferrarin, M., Rizzone, M., Lopiano, L., Recalcati, M., & Pedotti, A. (2004). Effects of subthalamic nucleus stimulation and L-dopa in trunk kinematics of patients with Parkinson's disease. *Gait & Posture*, *19*, 164–171.

Follett, K., Weaver, F., Stern, M., Marks, W., Hogarth, P., Holloway, K., Bronstein, J., Duda, J., Horn, S., & Lai, E. (2005). Multisite randomized trial of deep brain stimulation. *Archives of Neurology*, *62*, 1643–1644.

Hashimoto, T., Elder, C. M., Okun, M. S., Patrick, S. K., & Vitek, J. L. (2003). Stimulation of the subthalamic nucleus changes the firing pattern of pallidal neurons. *Journal of Neuroscience*, *23*, 1916–1923.

Humphries, M. D., Stewart, R. D., & Gurney, K. N. (2006). A physiologically plausible model of action selection and oscillatory activity in the basal ganglia. *Journal of Neuroscience*, *26*, 12921–12942.

Kita, H., Tachibana, Y., Nambu, A., & Chiken, S. (2005). Balance of monosynaptic excitatory and disynaptic inhibitory responses of the globus pallidus induced after stimulation of the subthalamic nucleus in the monkey. *Journal of Neuroscience*, *25*, 8611–8619.

Krack, P., Pollak, P., Limousin, P., Benazzouz, A., Deuschl, G., & Benabid, A. L. (1999). From off-period dystonia to peak-dose chorea—The clinical spectrum of varying subthalamic nucleus activity. *Brain*, *122*, 1133–1146.

Leblois, A., Boraud, T., Meissner, W., Bergman, H., & Hansel, D. (2006). Competition between feedback loops underlies normal and pathological dynamics in the basal ganglia. *Journal of Neuroscience*, *26*, 3567.

Lewis, M. M., Slagle, C. G., Smith, A. B., Truong, Y., Bai, P., McKeown, M. J., et al. (2007). Task specific influences of Parkinson's disease on the striato-thalamo-cortical and cerebello-thalamo-cortical motor circuitries. *Neuroscience*, *147*, 224–235.

Lozano, A. M., Dostrovsky, J., Chen, R., & Ashby, P. (2002). Deep brain stimulation for Parkinson's disease: Disrupting the disruption. *Lancet Neurology*, *1*, 225–231.

Maurer, C., Mergner, T., Xie, J., Faist, M., Pollak, P., & Lucking, C. H. (2003). Effect of chronic bilateral subthalamic nucleus (STN) stimulation on postural control in Parkinson's disease. *Brain*, *126*, 1146–1163.

McIntyre, C. C., Grill, W. M., Sherman, D. L., & Thakor, N. V. (2004). Cellular effects of deep brain stimulation: Model-based analysis of activation and inhibition. *Journal of Neurophysiology*, *91*, 1457–1469.

Mink, J. W. (1996). The basal ganglia: Focused selection and inhibition of competing motor programs. *Progress in Neurobiology*, *50*, 381–425.

Montgomery Jr, E. B., & Baker, K. B. (2000). Mechanisms of deep brain stimulation and future technical developments. *Neurological Research*, *22*, 259–266.

Nambu, A. (2004). A new dynamic model of the cortico-basal ganglia loop. *Progress in Brain Research*, *143*, 461–466.

Ogura, M., & Kita, H. (2000). Dynorphin exerts both postsynaptic and presynaptic effects in the globus pallidus of the rat. *Journal of Neurophysiology*, *83*, 3366–3376.

Okun, M. S., & Foote, K. D. (2005). Subthalamic nucleus vs globus pallidus interna deep brain stimulation, the rematch will pallidal deep brain stimulation make a triumphant return? *Archives of Neurology*, *62*, 533–536.

Ostergaard, K., & Sunde, N. A. (2006). Evolution of Parkinson's disease during 4 years of bilateral deep brain stimulation of the subthalamic nucleus. *Movement Disorders*, *21*, 624–631.

Pascual, A., Modolo, J., & Beuter, A. (2006). Is a computational model useful to understand the effect of deep brain stimulation in Parkinson's disease? *Journal of Integrative Neuroscience*, *5*, 541–559.

Perlmutter, J. S., & Mink, J. W. (2006). Deep brain stimulation. *Annual Review of Neuroscience*, *29*, 229–257.

Plenz, D., & Kitai, S. T. (1999). A basal ganglia pacemaker formed by the subthalamic nucleus and external globus pallidus. *Nature*, *400*, 677–682.

Raz, A., Vaadia, E., & Bergman, H. (2000). Firing patterns and correlations of spontaneous discharge of pallidal neurons in the normal and the tremulous 1-methyl-4-phenyl-1,2,3,6-tetrahydropyridine vervet model of parkinsonism. *Journal of Neuroscience*, *20*, 8559–8571.

Redgrave, P., Prescott, T. J., & Gurney, K. (1999). The basal ganglia: A vertebrate solution to the selection problem. *Neuroscience*, *89*, 1009–1023.

Rizzone, M., Ferrarin, M., Pedotti, A., Bergamasco, B., Bosticco, E., Lanotte, M., et al. (2002). High-frequency electrical stimulation of the subthalamic nucleus in Parkinson's disease: Kinetic and kinematic gait analysis. *Neurological Sciences*, *23*, S103–S104.

Rocchi, L., Chiari, L., Cappello, A., Gross, A., & Horak, F. B. (2004). Comparison between subthalamic nucleus and globus pallidus internus stimulation for postural performance in Parkinson's disease. *Gait & Posture*, *19*, 172–183.

Rocchi, L., Chiari, L., & Horak, F. B. (2002). Effects of deep brain stimulation and levodopa on postural sway in Parkinson's disease. *Journal of Neurology, Neurosurgery, and Psychiatry*, *73*, 267–274.

Rodriguez-Oroz, M. C., Obeso, J. A., Lang, A. E., Houeto, J. L., Pollak, P., Rehncrona, S., et al. (2005). Bilateral deep brain stimulation in Parkinson's disease: A multicentre study with 4 years follow-up. *Brain*, *128*, 2240–2249.

Rubin, J. E., & Terman, D. (2004). High frequency stimulation of the subthalamic nucleus eliminates pathological thalamic rhythmicity in a computational model. *Journal of Computational Neuroscience*, *16*, 211–235.

Stanford, I. M., & Cooper, A. J. (1999). Presynaptic μ and δ opioid receptor modulation of GABAA IPSCs in the rat globus pallidus in vitro. *Journal of Neuroscience*, *19*, 4796–4803.

Stefani, A., Fedele, E., Galati, S., Pepicelli, O., Frasca, S., Pierantozzi, M., et al. (2005). Subthalamic stimulation activates internal pallidus: Evidence from cGMP microdialysis in PD patients. *Annals of Neurology*, *57*, 448–452.

Stefani, A., Fedele, E., Galati, S., Raiteri, M., Pepicelli, O., Brusa, L., Pierantozzi, M., Peppe, A., Pisani, A., & Gattoni, G. (2006). Deep brain stimulation in Parkinson's disease patients: Biochemical evidence. *Journal of Neural Transmission. Supplementa*, *70*, 401–408.

Terman, D., Rubin, J. E., Yew, A. C., & Wilson, C. J. (2002). Activity patterns in a model for the subthalamopallidal network of the basal ganglia. *Journal of Neuroscience*, *22*, 2963–2976.

Vitek, J. L. (2002). Mechanisms of deep brain stimulation: Excitation or inhibition. *Movement Disorders*, *17*, S69–S72.

Vitek, J. L., Hashimoto, T., Peoples, J., DeLong, M. R., & Bakay, R. A. E. (2004). Acute stimulation in the external segment of the globus pallidus improves parkinsonian motor signs. *Movement Disorders*, *19*, 907–915.

Weaver, F., Follett, K., Hur, K., Ippolito, D., & Stern, M. (2005). Deep brain stimulation in Parkinson disease: A metaanalysis of patient outcomes. *Journal of Neurosurgery*, *103*, 956–967.

Yokoyama, T., Sugiyama, K., Nishizawa, S., Yokota, N., Ohta, S., & Uemura, K. (1999). Subthalamic nucleus stimulation for gait disturbance in Parkinson's disease. *Neurosurgery*, *45*, 41–47.